Magnetic response of isolated Cd impurities on ferromagnetic Ni surfaces and Ni-Pd interfaces: Access to ordered structures of polarized impurities with ultrahigh density

K. Potzger, A. Weber, W.-D. Zeitz, and H. H. Bertschat
Bereich Strukturforschung, Hahn-Meitner-Institut Berlin GmbH, D-14109 Berlin, Germany

M. Dietrich
Technische Physik, Universität des Saarlandes, D-66041 Saarbrücken, Germany
and The ISOLDE - Collaboration, CERN, CH-1211 Genève 23, Switzerland
(Received 4 March 2005; published 24 August 2005)

The induced *s* electron polarization at isolated Cd atoms on ferromagnetic Ni surfaces and the Pd/Ni interface was studied by the measurement of magnetic hyperfine fields (B_{hf}) applying perturbed angular correlation spectroscopy. For Cd on Ni, we found a surprisingly strong dependence of the B_{hf} values on the local geometry in terms of the number of nearest neighbors (NNs) leading to the conclusion that impurities with their nearest neighbors form magnetic clusterlike units embedded in the two-dimensional ferromagnetic surface. At the Pd/Ni interface, the B_{hf} values depend also on the stoichiometry (mixed NNs) due to the induced magnetic polarization of the Pd neighbors. Within the incommensurable unit cells of one monolayer of Pd on Ni, the impurities occupy selected sites. This observation might serve as a basis for the preparation of ordered structures with ultrahigh density of isolated impurities on patterned ferromagnetic substrates. The experiments prompted theoretical studies, which explain the coordination number dependence by the change of the density of polarized *s* states at the Fermi level from site to site.

DOI: 10.1103/PhysRevB.72.054435 PACS number(s): 75.70.Rf, 73.20.Hb, 76.80.+y

I. INTRODUCTION

Low dimensional magnetic structures are believed to offer great potential as high-density storage devices, switches, or sensors in data processing. For the last two decades, two-dimensional magnetic multilayer systems have been of special interest in physical research. Multilayer systems which exhibit the giant magnetoresistance effect[1] are already in commercial use, e.g., as spin valves. Recently, the analysis of the magnetic properties of zero-dimensional systems, like small Fe or Co clusters *attached* to Ni[2] or Pt surfaces,[3] came into the focus of interest. Especially the interactions between small structures consisting of ferromagnetic *d* metals and noble *d* metals like Pt or Pd are intensely investigated topics of basic research on the way to high-density data storage. As early as 1984, integral measurements of the increase of the magnetic moment of Pd-Ni(111)-layered systems were performed by U. Gradmann *et al.*[4] The increase was attributed to the induced magnetic polarization of Pd; this assumption was later confirmed in a local measurement.[5] In theoretical works by Blügel[6] and Dederichs *et al.*,[7] calculations were presented of magnetic moments induced in atomic Pd layers forming an interface with ferromagnetic materials. From calculations for a model system consisting of a Pd(001) single crystal covered by one monolayer of Ni, even an enhanced magnetic moment of the Ni layer was predicted.[6]

Following the trend of miniaturization, the ultimate goal of ongoing efforts in surface and interface science is the realization of regular arrays of magnetic units (clusters) consisting of a few atoms or even only one atom carrying one informational bit. There are several ways for the realization of such small structures, e.g., the use of pre-patterned surfaces showing a regular array of distinct surface sites (steps, strained areas,[8] or incommensurable terraces) for subsequently deposited atoms or clusters. The deposited material may act as a magnetic carrier for the information by including the nearest neighbors of the substrate.

One way to investigate such low-dimensional systems with atomic resolution is based on the use of radioactive probe atoms, which are deposited onto the surface or positioned at the interface. Such nuclear methods provide an extremely high sensitivity; for instance, perturbed angular correlation (PAC) spectroscopy, the main analysis tool in the present study, needs a total of atomic probe atoms between 10^{-4} and 10^{-6} of one atomic monolayer for a sample of one cm^2 surface size. At such a low concentration the impurities do not disturb the overall properties of the magnetic layer or the interface. Moreover, investigation of *d* metals using nuclear methods yields very local information involving only the first and, to a small extent, the second shell of nearest neighbors due to the localized character of the host *d* electrons.

The aim of this work was the determination of magnetic hyperfine fields (B_{hf}) as a measure for the *s*-electron polarization by host *d* electrons at Cd probe atoms positioned at locally different surface sites on uncovered flat Ni(111) or vicinal Ni(53,47,50) surfaces[9] and at the Pd/Ni(111) interface. In particular, the dependence of the induced magnetic properties of the impurity on the number, stoichiometry, and symmetry of nearest-neighbor atoms was a main point of interest. The particular positions of the probe atoms were identified by means of the electric field gradient (EFG) which was measured simultaneously along with the B_{hf} values.

Earlier investigations on structural (and magnetic) properties of probe atoms deposited onto the surface of Pd(001),[10]

Pd(111),[11] Ni(001),[12,13] and Ni(111),[9,12] as well as the investigation of ultrathin Pd layers on Ni(001),[5] were particularly helpful for the present work. Moreover, calculations of the EFG and the B_{hf} of probe atoms located at the Ni single crystal (s.c.) surface, performed by Lindgren and co-workers,[14,15] Mavropoulos,[16] Cottenier *et al.*,[17] and Bellini *et al.*[18] offered a substantial basis for the interpretation of the experimental data.

In the course of this paper we first illustrate the preparation of the samples and the deposition procedure for the radioactive probe atoms (Sec. II). In Sec. III, a short introduction will be presented into hyperfine interactions and into theoretical and experimental fundaments of the PAC spectroscopy to the extent that it is needed for the combined interaction. In Sec. IV and V, the results of the experiments are discussed. The conclusions follow in Sec. VI.

II. SAMPLE PREPARATION AND DEPOSITION OF RADIOACTIVE ISOTOPES

The experiments were performed in the UHV chamber (base pressure 2×10^{-9} Pa) ASPIC (Apparatus for Surface Physics and Interfaces at CERN). The samples were commercial 1-mm-thick cylindrically (10 mm diameter) shaped Ni(111) and vicinal Ni(53,47,50) single crystals. In the ASPIC chamber, the sample's surface was cleaned and smoothed in a repetitive procedure by Ar sputtering ($I=7$–$10\ \mu A, E=0.7$–1 keV) and annealing ($T=1000$–1200 K). Surface contamination and structural quality were controlled by Auger electron spectroscopy (AES) and low-energy electron diffraction (LEED), respectively.

For an efficient deposition of the radioactive probe atoms onto the sample surface without breaking the vacuum, ASPIC is directly connected by a UHV beam line to the on-line mass separator ISOLDE (isotope separator online device) at CERN. The mass separator delivers a variety of radioactive nuclei suitable for PAC in a sufficient amount for solid-state investigations. The isotopes are produced by bombarding a target with a pulsed proton beam (pulse length 2.4 μs) at an energy of about 1 Gev.[19] The resolution of the mass separating magnet is given by $\Delta m/m=1/2400$, i.e., the ISOLDE mass separator provides extreme clean isotope beams, suitable for surface and interface investigations. A further advantage of the direct connection of the UHV-chamber ASPIC to ISOLDE is the availability of short-lived isotopes. In our experiment, the nuclear probes ^{111m}Cd($t_{1/2}=49$ min) or ^{111}In($t_{1/2}=2.83$ d), decaying to the PAC probe ^{111}Cd were used. The decay scheme and nuclear properties of the probe isotopes are shown in Fig. 1.

In the prechamber of ASPIC, the radioactive isotopes delivered by the mass separator ISOLDE are initially implanted with an energy of 60 keV into a carefully pre-cleaned Mo catcher foil. In a two step process, the probe atoms are transferred to the main chamber of ASPIC and evaporated onto the sample surface. It is due to the two-step process that unwanted contamination of the sample surface can be kept to less than 2%. Dependent on the structure of the sample surface, the probes are able to occupy stable adsorption sites after deposition. While a Ni(111) s.c. surface offers large

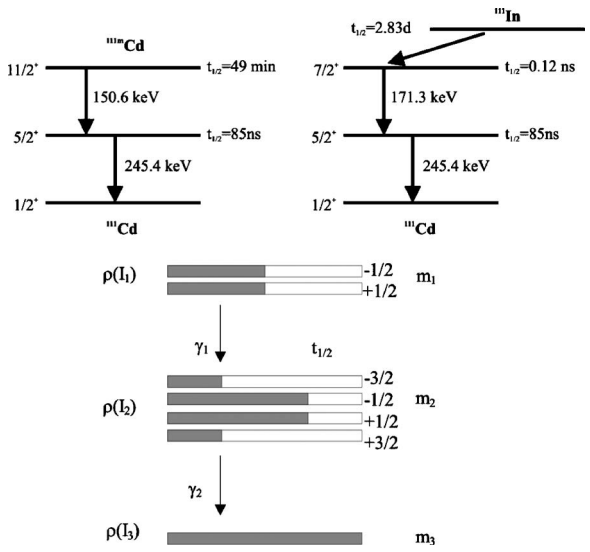

FIG. 1. Decay scheme of ^{111m}Cd/^{111}Cd and ^{111}In/^{111}Cd (data taken from Ref. 31). Lower part: Schematic representation of a $\gamma\gamma$ cascade. The gray lines indicate the (selected) population of the sub states leading to an anisotropy of the $\gamma\gamma$ correlation.

terraces, a vicinal Ni(53,47,50) s.c. surface shows a regular array of steps suitable for the preparation of low-symmetry adsorption sites (Fig. 2). There is clear evidence for a regular step array after several sputtering and annealing steps by LEED. Due to the step array with periodicity much lower than for the Ni(111) unit cell, the reciprocal-space vectors split and that could be detected by LEED for the as-prepared sample [Fig. 2(b)]. Minimizing the step-free energy cusps and edges are believed to be formed due to the cut direction [conceptional view in Fig. 2(c)], since their existence is also evident from the results of the experiments presented here (Sec. IV).

If positioned at a specific site, the nucleus of the probe atom experiences electric and magnetic hyperfine interactions dependent on the *number* of the nearest-neighbor atoms. The aim in preparation before recording the PAC spectrum is to force the probe atoms to occupy—in the optimal case—only one kind (fraction) of uniform sites, since a numeric resolution of a PAC spectrum containing more then three different fractions corresponding to an occupation of three different surface sites is, in general, rather difficult. Mainly two methods for the preparation of uniform surface sites were applied as described in the following two paragraphs.

After deposition of the radioactive probe atoms, the sample was annealed at a chosen temperature. Diffusion of the probe and surface atoms leads to a predominant occupation of the desired surface sites by the probe atoms. A theoretical analysis of the diffusion behavior of In atoms on a transition-metal surface (here Cu) was performed by van Siclen.[20] The author calculated the migration energies for In atoms following various diffusion paths. It was found that these energies are low for paths across the terrace or along the step in comparison with "exchange mechanism" paths leading to substitutional sites. Concordantly, earlier and present experimental studies on the diffusion of radioactive

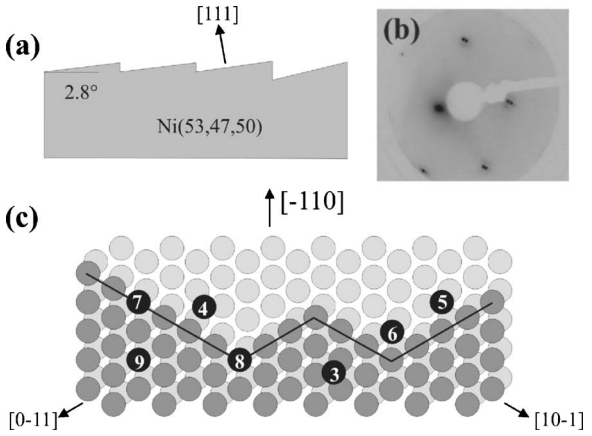

FIG. 2. (a) Schematic side view of the Ni(53,47,50) vicinal surface corresponding to a Ni(111) surface cut in the [−1 1 0] direction at an angle of 2.8°. Steps arising from the cut are indicated. (b) LEED pattern of a Ni(53,47,50) surface at $E=147$ eV after preparation. The splitting of the (111) reflexes clearly indicates a regular step array with steps following the [−1 1 0] direction as indicated in (c). Since the step edges are of high free energy, a breakup into zigzaglike lateral sub steps is expected. (c) Model of the step edge: Due to the minimization of the surface free energy, the formation of edges and cusps is most probable. Geometrically possible adsorption sites of isolated atoms are conceptionally shown and indicated (•). The numbers of nearest Ni neighbors are mentioned for each adsorption site. A substitutional terrace (C_{3v} symmetry) corresponds to 9, a substitutional kink site (C_1) to 8, a substitutional step site (C_{1s}) to 7, a free kink site to 6 (C_1), a free step site (C_{1s}) to 5 or 4, a free terrace (adatom) site (C_{3v}) to 3 nearest neighbors. Note the pecularity that steps along the [0 −1 1] direction offer only sites with NN=5, whereas steps along the [1 0 −1] direction also offer sites with NN=4, which we call "distant step sites" (see Table I).

^{111}In and ^{111m}Cd probes show for the site occupation that at low temperatures mainly adatom sites [<120 K for Pd(111),[11] 36 K for Ni(111),[9] and 77 K for Ni(001) (Ref. 12)] or free step and kink sites [80–320 K for Pd(111),[11] and 120–250 K for Ni(001) (Ref. 12)] and at higher temperatures mainly substitutional step sites [250–400 K for Pd(111),[11] and above 470 K for Ni(001) (Ref. 13)] and substitutional terrace sites [above 370 K for Pd(111),[11] and above 470 K for Ni(001) (Ref. 13)] are occupied.

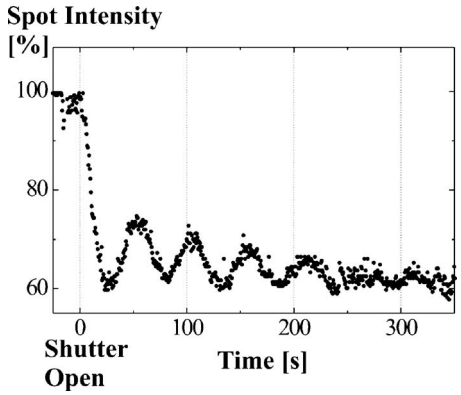

FIG. 3. Medium-energy electron diffraction (MEED) spectrum of Pd growth on Pd(001) at $T=300$ K. The growth time for one monolayer amounts to 51 s with the chosen set of parameters for the MBE gun.

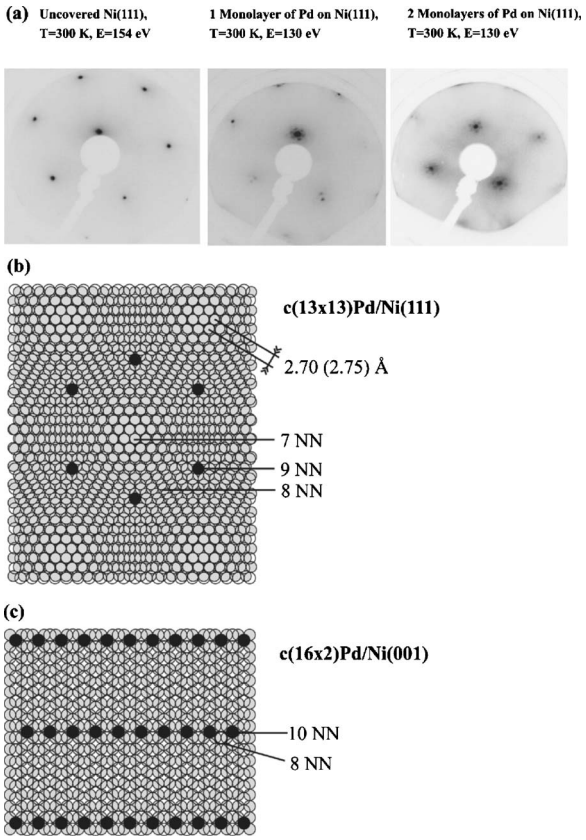

FIG. 4. (a)LEED pattern of an uncovered and Pd covered Ni(111) surface. (b) Schematic view onto an atomic monolayer of $c(13\times13)$Pd on Ni(111). The distance of nearest neighbors in the Pd layer (2.70 Å) almost equals the corresponding distance at a Pd(111) s.c. surface (2.75 Å). The Moiré pattern offers sites, where surface atoms have seven, eight and nine nearest neighbors (the latter shown as black circles). (c) Schematic view onto an atomic monolayer of $c(16\times2)$Pd on Ni(111). The incommensurate pattern offers sites where surface atoms have eight, nine and ten nearest neighbors (the latter shown as black circles).

Substitutional terrace sites have been prepared by decorating the surface with an ultrathin film *after* deposition of the probe atoms. In the present work, heteroepitaxy was performed producing ultrathin Pd films on Ni(111) rather then homoeptaxy.[13] The growth time for one monolayer of Pd on Pd(001) was adjusted to the parameters of the evaporation cell using medium-energy electron diffraction (MEED) as presented in Fig. 3. The LEED analysis of the growth structure on Ni(111) and Ni(53,47,50) exhibits an incommensurate $c(13\times13)$Pd unit cell. This finding agrees with scanning tunneling microscopy (STM) measurements of Terada *et al.*[21] Moreover, it was found that at room temperature Pd grows in the Stranski-Krastanov mode initially decorating the Ni(111) surface steps. The Pd monolayer becomes unstable at temperatures above 380 K. LEED patterns for different Pd coverage are shown in Fig. 4(a). As shown in Fig. 4(b), the atomic Pd layer along with the topmost Ni layer form a Moiré pattern in principle offering different numbers of nearest neighbors (NNs) for impurities within the Pd

monolayer. A periodic vertical corrugation is present, as can be deduced from the LEED pattern. From a hard-sphere model, the amplitude amounts to 0.4 Å.

III. HYPERFINE INTERACTIONS AND PAC MEASUREMENT

Nuclei of probe atoms located on a ferromagnetic surface or layer experience combined, i.e., electric and magnetic hyperfine interactions. The electric quadrupole moment and magnetic dipole moment, which are inherent properties of the nucleus in the particular excited state (with spin I and half life $T_{1/2}$), interact with the EFG and B_{hf}, respectively, arising from the surrounding charges and polarized electrons, respectively. The hyperfine interactions are described in more detail in the following section.

A. Electric quadrupole interaction

The electric quadrupole interaction is the first non vanishing ($l=2$) contribution in a multipole expansion of the electrostatic interaction energy

$$W_{el} = \frac{\int \rho_e(r)\rho_n(R)}{|r-R|} = \sum_l 4\frac{\pi}{2l+1}\sum_{m=-l}^{l} Q_{lm}\Phi_{lm}^*$$

between an atomic nucleus with charge distribution ρ_n and its surrounding charge distribution ρ_e.[22] It describes the energy of a quadrupole $[Q_{2m}=\int R^2\rho_n(R)Y_{2m}d^3R=ZR^2Y_{2m}]$ at the origin exposed to an electric-field gradient or EFG $\{\Phi_{2m}^*=\int[\rho_e(r)/r^3]Y_{2m}^*d^3r\}$. In Cartesian coordinates of the principal axes system, the EFG is well described by the set

$$(V_{zz}, \eta, \alpha, \beta, \gamma), \tag{1}$$

where $V_{ii}=\Phi_{ii}-\frac{1}{3}\Delta\Phi$ is a traceless expression for the EFG value. The asymmetry parameter is given by

$$\eta = (V_{xx}-V_{yy})/V_{zz}. \tag{2}$$

The Euler angles α, β, γ define the orientation of the EFG within the laboratory coordinate system.

The quadrupole interaction lifts the degeneracy of the magnetic spin quantum number of the nucleus. The transitions between the energy levels are described by the electric quadrupole interaction frequency

$$\omega_Q = \frac{eQV_{zz}}{4I(2I-1)}. \tag{3}$$

In solid-state physics, the ansatz for V_{zz} is as follows:[14]

$$V_{zz} = V_{zz}(\text{el}) + V_{zz}(\text{ion}), \tag{4}$$

where V_{zz} (ion) represents the contribution of the positive ion cores and

$$V_{zz}(\text{el}) \sim e\int \rho_e(R)\frac{3\cos^2\theta-1}{r^3}drd\theta d\varphi \tag{5}$$

is the dominant contribution from the density of electronic states. The EFG decreases proportionally to r^3 which means that the electric quadrupole interaction is of very short range. Since the EFG originates from a nonspherical distribution of electric charges near the probe nucleus, it is governed by the character of the electronic bonds and the number and arrangement (symmetry) of the nearest-neighbor atoms. At the majority of metal surfaces, the behavior—large V_{zz}=high NN and low V_{zz}=low NN—is assumed to be a general tendency. This was recently supported by calculations of Lindgren[15] and Cottenier *et al.*[17] The asymmetry parameter η and the orientation of the EFG (α, β, γ) depend on the symmetry of the local neighborhood of the probes. At surfaces, full rotational symmetry C_{3v} or C_{4v} leads to $\eta=0$, while the orientation of the EFG points along the surface normal. Lower symmetry groups like C_{2v} present at (110) oriented surfaces or C_{1s} symmetry at steps yield $\eta\neq 0$ and the orientation deviates from the surface normal. The parameters of the EFG offer a powerful tool to identify the surface site of the probe atoms on or in the surface or interface.[14–17]

B. Magnetic dipole interaction

The first-order energy term for the interaction[22] between the nuclear magnetic dipole moment $\mu=\mu_N g_I I$ (μ_N is the Bohr nuclear magneton, g_I is the nuclear Landé factor) and the magnetic hyperfine field B_{hf} is given by

$$(W_{mag})_{Im} = \langle \text{Im}|-\mu_z B_{hf}|\text{Im}\rangle = -\mu_N g_I m B_{hf} = m\ \omega_L. \tag{6}$$

The Larmor frequency ω_L represents the transition frequency between two neighboring m substates of the nuclear spin I.

In general, B_{hf} consists of dipolar and orbital contributions, and the Fermi-contact field.[23] For $4sp$ and $5sp$ elements in ferromagnetic transition metals, the major contribution to the magnetic hyperfine field is given by the Fermi contact term, determined by the magnetic moment produced by the s-electron density.[24] It is proportional to the difference between s-minority ($\downarrow$) and s majority ($\uparrow$) electrons, called s-spin density $\rho_{Spin}(s)$. The magnetic contact interaction energy is given by[23]

$$E_{Fermi} = -\frac{2\mu_0}{3}\mu_e\rho_{Spin}\delta(r). \tag{7}$$

While the magnetic dipole interaction and the orbital term decrease proportional to r^3, the dominant Fermi contact field has no spatial extension. The spatial range of the magnetic hyperfine interaction at the probe nucleus therefore is limited to the first and, to a small extent, to the second shell of neighboring atoms, since the exchange splitting of the s states is caused by the hybridization with spin-split electronic d states, which are localized close to their parent transition-metal atom.

C. Combined interaction

For probe atoms which are positioned at non cubic sites (e.g., at surfaces or interfaces) of magnetic materials, combined magnetic dipole and electric quadrupole interactions are present. The combined interaction is rather complex and

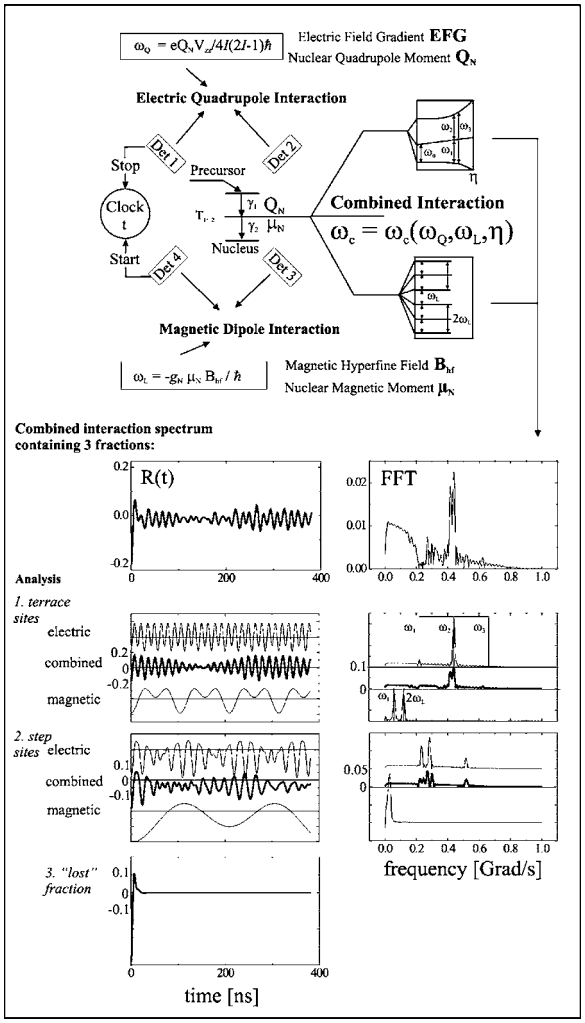

FIG. 5. Representation of the combined magnetic dipole and electric quadrupole interaction. As an example, the composition of a PAC spectrum from three fractions of combined interaction frequencies is shown schematically. The EFG and B_{hf} values are chosen to be typical for probe atoms located at substitutional *terrace sites* (first fraction):$[|V_{zz}|=11.6\times10^{17}(V/\mathrm{cm}^2), \eta=0, \alpha=\beta=\gamma=0°]$,$(|B_{hf}|=4.1\ T, \theta=90°, \varphi=0°)$and *step sites* (second fraction) of a ferromagnetic surface:$[|V_{zz}|=8.2\times10^{17}(V/\mathrm{cm}^2), \eta=0, \alpha=0°, \beta=30°, \gamma=0°]$,$(|B_{hf}|=1T, \theta=90°, \varphi=0°)$.Finally, they are combined in a joint $R(t)$ time spectrum of both fractions (25% each) along with a third ("lost") fraction of 50% originating from sites with a broad distribution of hyperfine parameters (surface defects, contamination).

leads to a nuclear state splitting depending on B_{hf} and its orientation (θ, φ) with respect to the EFG orientation and the EFG parameters.[25] The electric quadrupole and magnetic dipole interaction frequencies ω_Q and ω_L are measured simultaneously in the combined interaction frequency

$$\omega_C = \omega_C(B_{hf}, \theta, \phi, V_{zz}, \eta, \alpha, \beta, \gamma). \tag{8}$$

A schematic illustration of the combined interaction is given in Fig. 5.

D. Perturbed angular correlation (PAC) spectroscopy

The theory of PAC spectroscopy is well described.[26–29] The most important features are summarized as follows: For PAC spectroscopy, usually radioactive isotopes are used, which decay in a $\gamma\gamma$ cascade populating and depopulating an isomeric state of I_2 (Fig. 1). Assuming an axially symmetric perturbing interaction to be present (hyperfine interaction as described in Secs. III A–III C) and using the nomenclature of the Liouville space,[27] the density operator of the state I_2 becomes time dependent:

$$\rho(I_2,t) = G(\omega_C t) D(\gamma_1 \rightarrow z) \rho(I_2, t=0), \tag{9}$$

with the perturbation superoperator $G(\omega_C t)$ and the interaction frequency ω_C for the general case of combined interaction. The rotation operator D transforms the (aligned) density operator $\rho(I_2, t=0)$ into the basis of the interaction.

The transition probability from the state I_2 to the state I_3 via emission of the gamma photon γ_2 (Fig. 1) depends on the emission angle and the final sub states m_3 of the final angular momentum I_3. It is given by the distribution operator $W(\gamma_2)$. The time-dependent perturbed angular correlation function $W(\gamma_1, \gamma_2, t)$ as the expectation value of $W(\gamma_2)$ with respect to $\rho(I_2, t)$ is given by

$$W(\gamma_1,\gamma_2,t) = \sum_{\lambda,q,\lambda',q'} \frac{A_{\lambda\lambda'}}{\sqrt{2\lambda+1}\sqrt{2\lambda'+1}} Y_q^{+\lambda}(\theta_1,\phi_1) \times G_{qq'}^{+\lambda\lambda'}(-\omega_C t) Y_{q'}^{\lambda'}(\theta_2,\phi_2), \tag{10}$$

where $A_{\lambda\lambda'}$ is the anisotropy coefficient and G is the perturbation operator given by

$$G_{qq'}^{\lambda\lambda'} = \delta_{qq'} \sqrt{(2\lambda+1)(2\lambda'+1)} \sum_{m_2 m_2'} \begin{pmatrix} I_2 & \lambda & I_2 \\ -m_2 & q & m_2' \end{pmatrix} \times e^{i(E_{m_2} - E_{m_2'})t} \begin{pmatrix} I_2 & \lambda' & I_2 \\ -m_2 & q & m_2' \end{pmatrix}. \tag{11}$$

The expressions in the parentheses are Wigner $3j$ symbols.

E. PAC time spectra

The correlation function [Eq. (10)] enters the coincidence count rate C_{ij} between the γ detectors i and j in the following way:

$$C_{ij}(\gamma_1,\gamma_2,t) = C_0 \exp(-t/\tau) W(\gamma_1,\gamma_2,t) + B. \tag{12}$$

TABLE I. Experimental results for ^{111}Cd on pure Ni

NN[a]	Location[b]	Ni-surface orientation	$\lvert V_{zz}\rvert$ (10^{18} V/cm^2)	η	α,β,γ (°)	FWHM[c] (%)	$\lvert B_{hf}\rvert$ (T)	Experiment[d] or Ref.	Fraction[e] (%)
12	bulk						−6.69(3)	Ref. 37	
9	terrace	(111)	1.23 (3)	0.00 (5)	0, 0, 0 (10)	2.0 (5)	6.6 (2)	E_1	45
9	terrace	(111)	1.13 (5)	0.00 (5)	0, 0, 0 (10)	4.0 (5)	6.2 (4)	E_2	40
9	terrace	(111)	1.14 (at 77 K)				6.7 (1)	Ref. 12	
8	terrace	(001)	0.82 (2)	0.00 (5)	0, 0, 0 (10)		3.5 (4)	Ref. 13	
7	*s* step	(111)	0.73 (2)	0.72 (6)	-, 20 (10),-	0.0 (5)	4.1 (2)	E_2	15
7	*s* step	(001)	0.73 (2)	0.6 (2)	-, 35 (8),-		3.9 (4)	Ref. 13	
6	*f* kink	(111)	0.61 (2)	0.30 (5)	±18 (8), 32 (8), 0	1.0 (5)	0.8 (3)	E_3	22
6	*f* kink	(111)	0.61 (2)	0.30 (5)	±20 (20), 20 (10), 0	0.0 (5)	1.0 (4)	E_4	8
5	*f* step	(111)	0.67 (2)	0.26 (8)	±35(20), −38(10), 90	1.0 (5)	3.9 (3)	E_3	17
5	*f* step	(111)	0.67 (2)	0.26 (8)	±40 (25), −48(8), 90	1.0 (5)	4.3 (3)	E_4	22
5	*f* step	(111)	0.67 (5)	0.11 (5)	β=53(5)		4.5 (5)	Ref. 32	
4	d.f. step	(111)	4.8 (5)	0.9 (1)	0, 25 (5), 0		8.1 (5)	Ref. 32	
4	adatom	(001)	0.27 (3)	0.1 (1)	0,0,0		7.3 (2)	Ref. 12	
3	adatom	(111)	0.10 (5)	0.1 (1)	0, 0, 0 (15)	2.0 (5)	16.0 (8)	E_5, Ref. 9	50
3	adatom	(111)	0.19 (10)	0.1 (1)	0, 0, 0 (5)		14.0 (10)	Ref. 32	

[a]Number of nearest neighbors and/or coordination number.
[b]*s*=substitutional, *f*=free, d.f.=distant free.
[c]Full width at half maximum for the broadening of the combined interaction frequency (relative to the frequency total).
[d]Denomination of the experiment E_j.
[e]Percentage of the fraction defined by NN with respect to the full amount of decays.

B denotes the background and τ is the lifetime of the isomeric state. The PAC-time spectrum $R(t)$ is a ratio function measured in a four detector array (Fig. 5,top). It is given by the ratio of the count rate $C(\Theta)$ (Θ is the angle between the detectors) of the four-detectors as

$$R(t) = 2[C(180^\circ) - C(90^\circ)]/[C(180^\circ) + C(90^\circ)]. \tag{13}$$

In the general case, the $R(t)$ spectrum contains combined electric quadrupole and magnetic dipole interaction frequencies [Eq. (8)] resulting from more than one set of well defined (discrete) hyperfine parameters, e.g., if the probe atoms are distributed over adsorption sites with different local symmetry or different numbers of nearest neighbors.

The full amplitude of

$$R(t) = \sum_{n=1}^{N} f_i r_i(t) + f_l r_l(t) \tag{14}$$

representing the full amount of recorded coincidences for one experiment is composed of subamplitudes (fractions) f_i of the particular subspectra $r_i(t)$, where i denotes the number of nearest neighbors. Probe atoms having defects (e.g., contamination) in their local neighborhood contribute a broad distribution of interaction frequencies to the $R(t)$ spectrum. They add up to an average subspectrum $r_l(t)$ showing a strong damping, within a few ns. This "lost" fraction f_l plays no role for the evolution of the main part of the $R(t)$ spectrum with discrete frequencies. A numerical step by step composition of a typical spectrum ending at Eq. (13) is simulated in Fig. 5 using the DEPACK program of Lindgren.[30]

Within the experimental setup for the PAC measurement the sample is located on a manipulator inside the UHV chamber. The γ rays are emitted from the probe atoms located at the sample surface and detected using NaI scintillation crystals connected to photomultipliers. These four-detectors are arranged in standard 90 ° geometry. The sample normal is aligned perpendicular to the detector plane and at 45° to each of the detectors. The PAC time spectra are recorded by performing coincidence measurements of the two γ quanta emitted during the radioactive decay (Fig. 1) as start-, respectively stop-signals. The individual experiments are treated in the following section, where the discussion will be limited to the EFG, since its parameters are essential for the identification of the probe locations on the surface. B_{hf} will be treated in Sec. V.

IV. RESULTS

A. Probes at pure Ni-coordination numbers: ^{111}Cd on the Ni(111) surface

In the first series of experiments, we investigated the hyperfine interactions at Cd probe atoms located at different surface sites of a Ni(111) and a vicinal Ni(53,47,50) single crystal. Cd probes located at identical surface sites on a sample are considered as a fraction, defined by f_i [see Eq. (17)] for each experiment E_k (k denotes the number of the particular experiment in order to distinguish between different experiments with different preparation procedures). In

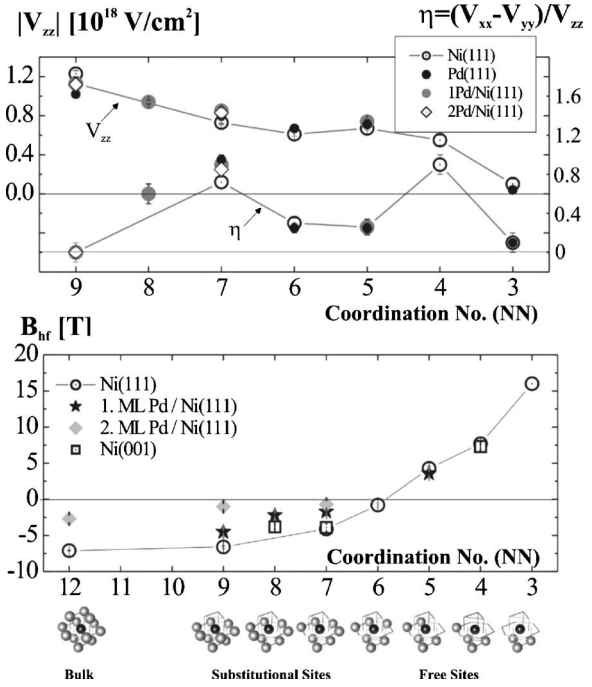

FIG. 6. Upper part: electric-field gradient V_{zz} and asymmetry parameter η at Cd located at different adsorption sites on Ni(111), Pd(111) (Ref. 13) and Pd covered Ni(111) surfaces. The x axis shows the adsorption site and the corresponding number of nearest neighbors NN. The value for NN=4 at Ni(111) was taken from Ref. 32. Lower part: magnetic hyperfine fields at Cd on an uncovered and Pd-covered Ni(111) single crystal. The Cd probes are located in the first or second layer but uncovered and at different adsorption sites, corresponding to a given number of nearest neighbors. The sign was not measured but was deduced from theoretical considerations. The B_{hf} values at Cd probe atoms on the Ni(001) surface were added from Refs. 12 and 13. The value for NN=12 was taken from Ref. 37 and the value for NN=4 at Ni(111) was taken from Ref. 32.

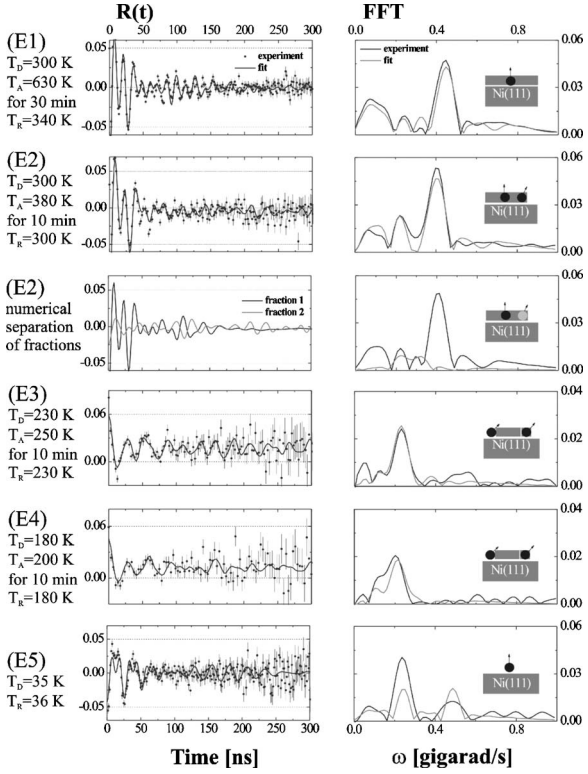

FIG. 7. PAC time spectra and fast-fourier transforms of experiments E_1-E_5 (see text) for ^{111}Cd on Ni(111) single-crystal surface. T_D, T_A, and T_R denote the deposition, annealing, and $R(t)$ recording temperature, respectively. A structural model is indicated. For E_2 the two fractions of probes were numerically split in a simulation.

Table I all experimentally obtained sets of hyperfine parameters at the ^{111}Cd probe atoms for the different sites, i.e., the different numbers of nearest neighbors (NNs) are presented. A graphic representation of the magnetic hyperfine fields (B_{hf}) and the electric-field gradients (EFG) is given in Fig. 6 The data are deduced from the $R(t)$ time spectra presented in Fig. 7 The particular measurements and the identification processes of the surface sites using the EFG are presented and discussed as follows, sorted by the number of nearest neighbors NN of the probe atoms.

1. NN=9 and NN=7

In order to observe probe atoms occupying substitutional surface sites with NN=9, two experiments (E_1, E_2) were performed: After deposition of the probe atoms, the Ni(111) sample was annealed at 630 K (E_1) and 380 K (E_2). The PAC time spectra (Fig. 7) for both experiments could be fitted assuming a fraction f_9 representing the substitutional terrace sites with NN=9. In E_2 an additional fraction f_7 occurs due to the lower annealing temperature. It could be identified as a substitutional step site with NN=7 (Fig. 2). For the identification of the surface site of the probe atoms belonging to a particular fraction, the EFG parameters [Eq. (2)) are used. For f_9 the asymmetry parameter η of the EFG is zero. It is symmetric in the xy plane as is expected for terrace sites. Due to the high annealing temperatures the occupation of adatom sites (where also $\eta=0$) is impossible for Cd. Comparing the value of the EFG parameters with theoretical calculations performed by Lindgren and co-workers[14,15] and more recently by Cottenier *et al.*,[17] we also find agreement with a substitutional terrace site with NN=9. Fraction $f_9(E_2)$ is much more damped and its V_{zz} is about 10% lower then for $f_9(E_1)$. This effect is assumed to originate from the lower annealing temperature, leading to a distribution of the probes within an area close to the edges of the terraces and thus showing more relaxation.

Fraction $f_7(E_2)$ shows a nonzero asymmetry parameter η of the EFG and the direction of the EFG deviates from the surface normal (Table I), which is typical for step sites. From the orientation of the EFG and comparison of its magnitude with earlier experiments for the Pd(111) surface,[11] the identification in terms of substitutional step sites with NN=7 becomes evident.

2. NN=6 and NN=5

In order to observe probe atoms occupying step sites, the vicinal Ni(53,47,50) single-crystal surface (symmetry group C_{1s} was used, since it offers an appropriate density of ori-

TABLE II. Experimental results for Pd-covered Ni surfaces.

NN[a]	Location in Pd	Coverage and surface orientation	$\lvert V_{zz}\rvert$ (10^{18} V/cm^2)	η	α,β,γ (°)	FWHM[b]	$\lvert B_{hf}\rvert$ (T)	Experiment[c] or reference	Fraction[d] (%)
12	2 ML	6 ML Pd/Ni(111)	0	0	0	0.25(5)	2.7 (5)	E_9	50
10	1 ML	1 ML Pd/Ni(001)	1.14 (2)	0.00 (5)	0, 0, 0		3.9 (2)	Ref. 5	
9	1 ML	1 ML Pd/Ni(111)	1.20 (3)	0.00 (5)	0, 0, 0 (10)	0,020(5)	4.5 (2)	E_6	40
9	1 ML	1 ML Pd/Ni(111)	1.13 (2)	0.00 (5)	0, 0, 0 (10)	0,020(5)	4.5 (2)	E_7	45
9	2 ML	2 ML Pd/Ni(111)	1.12 (3)	0.00 (5)	0, 0, 0 (8)	0,030(5)	1.0 (4)	E_8	60
9	2–6 ML	6 ML Pd/Ni(111)	1.12 (4)	0.00 (5)	0, 0, 0 (10)	0,030(5)	0 (+1)	E_9	10
8	1 ML	0.4 ML Pd/Ni(111)	0.94 (2)	0.6 (1)	±10 (10), 10 (5), 0	0,000(5)	2.2 (2)	E_{11}	20
7	1 ML	0.4 ML Pd/Ni(111)	0.85 (2)	0.85 (8)	±10 (10), 10 (10), 0	0,000(5)	1.6(2)	E_{11}	20
7	1 ML	0.4 ML Pd/Ni(111)	0.84 (2)	0.88 (8)	±20 (20), 20 (8), 0	0,010(5)	1.7 (2)	E_{10}	40
7	1 ML	0.4 ML Pd/Ni(111)	0.86 (2)	0.9 (1)	±20 (20), 20 (10), 0	0,010(5)	1.5 (3)	E_{12}	20
7	2 ML	1 ML Pd/Ni(111)	0.83 (3)	0.85 (8)	-, 20 (10),-	0,020(5)	0.9(5)	E_7	15
7	2 ML	1.8 ML Pd/Ni(111)	0.84 (3)	0.85 (8)	-, 20 (10), 0	0,025(5)	0.7 (5)	E_{13}	50
5	1 ML	0.4 ML Pd/Ni(111)	0.74 (2)	0.26 (8)	±20 (20), −55 (18); 90	0,010(5)	3.6 (3)	E_{12}	18

[a]Number of nearest neighbors and/or coordination number.
[b]Full width at half maximum for the broadening of the combined interaction frequency (relative to the frequency total) obtained from the damping parameters.
[c]Denomination of the experiment E_j.
[d]Percentage of the fraction defined by NN with respect to the full amount of decays.

ented steps for the probe atoms, while the surface terraces are still oriented in the (111) direction (Sec. II). In two experiments, the Ni sample was annealed at different temperatures after deposition of the ^{111m}Cd/^{111}Cd probes (Fig. 7). The spectrum of each experiment (E_3,E_4) could be fitted assuming only two fractions (f_5 and f_6) representing free step sites with NN=5 and free kink sites with NN=6.

The asymmetry parameter η for both fractions is nonzero as is expected from the low symmetry of step like sites. The direction of the EFG (Table I) allows us to distinguish between kink and step sites.

The amount of probes in each fraction reflects the diffusion behavior: the fraction of the higher coordinated kink sites (f_6) increases with higher T_A in comparison to the lower coordinated step sites (f_5) because the motion to kinks requires a higher activation energy. The coexistence of both kink and step sites on the Ni(53,47,50) surface supports the shape model presented in Fig. 2(c) (comp. Sec. II). A recent experiment by Prandolini *et al.*[32] showed that on Ni(53,47,50), also free step sites with NN=4 (which we call distant free step site, Table I) can be occupied at a lower temperature (39 K).

3. NN=3

Surface sites with C_{3V} symmetry are adatom sites on Ni(111) with NN=3. For the preparation of these sites in experiment E_5 the probes ^{111}In/^{111}Cd were not annealed after deposition at T_D=35 K. V_{zz} at these sites is smaller by a factor of about 10 than for substitutional sites, in agreement with the general trend described by Cottenier *et al.*[17] From geometrical considerations it could be expected that the isotopes occupy hcp-like as well as fcc-like surface sites. Since only one fraction (f_3) was found to fit the spectrum, either all isotopes occupy a hcp- or fcc-like adatom site or the differences in the EFG and B_{hf} between the two sites are too small to be resolved.

B. Probes at mixed Pd-Ni coordination numbers (NN): ^{111}Cd at the Pd/Ni(111) interface

In the second series of experiments, a varying amount of nearest-neighbor Ni atoms of the Cd probes was substituted by Pd atoms. This substitution was realized by decorating the Ni(111) surface in successive experiments with between 0.4 and 6 monolayers of Pd and allowing the deposited Cd probe atoms to occupy different sites within the Ni/Pd interface. The EFG and B_{hf} values determined in the experiments are presented in Table II and Fig. 6. The data were deduced from the $R(t)$ spectra presented in Figs. 8 and 9. A detailed presentation of the experiments follows. The nomenclature for the different experiments refers to Table II. The fractions are labeled using f_i^j, where i denotes the number of nearest Ni neighbors and j the number of nearest Pd neighbors.

1. NN=9—one monolayer of Pd

In order to prepare surface sites with NN=9, the probe atoms have to be brought into the terraces of one monolayer of Pd on Ni(111). Two different experiments were performed: in experiment E_6 one monolayer of Pd was evaporated onto ^{111}In atoms *already* located in terrace sites of a Ni(111) surface at T_E=200 K; and in E_7 the probes were evaporated *after* deposition of one monolayer of Pd and subsequently annealed at about 340 K; at 380 K the Pd layer becomes unstable.

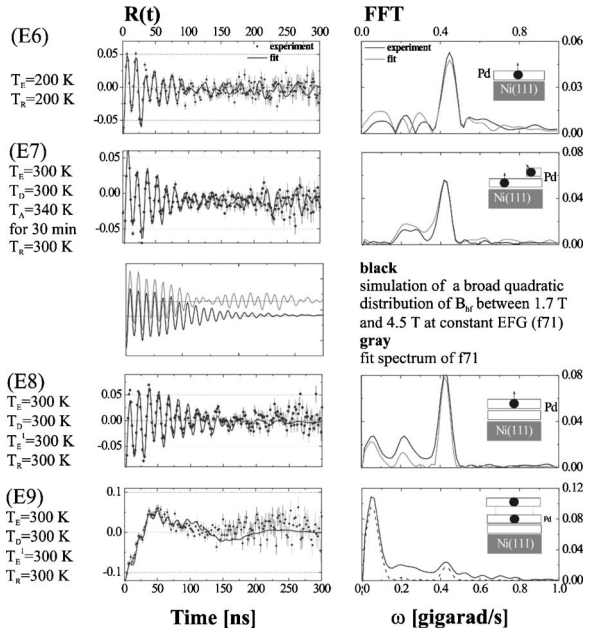

FIG. 8. PAC time spectra and the fast-fourier transforms (right graphs) of experiments E_6-E_9 (see text). T_D, T_A, and T_R denote the deposition, annealing and $R(t)$-recording temperature, respectively. A structural model is indicated. The figure contains a simulated spectrum of a broad distribution of the B_{hf} value between 4.5 and 1.7 T which corresponds to 9 or 7 NN. The EFG is taken as equal in order to demonstrate only the effect of the magnetic hyperfine field.

In spite of the incommensurate growth of the Pd layer (Fig. 4), leading to possible adsorption sites within the Pd terrace with undefined NNs ranging from NN=7 to NN=9, the PAC time spectra for both E_6 and E_7 contain large fractions of probe atoms which could be attributed to surface sites with a uniform number of nearest neighbors, because only discrete frequencies were measured.

The fraction f_3^6 present in both E_6 and E_7 was attributed to a substitutional terrace site with NN=9, since its EFG points along the surface normal and the asymmetry vanishes ($\eta=0$) indicating a surface site with full rotational symmetry. Moreover, the value of V_{zz} is close to that of the substitutional terrace sites on Ni(111) or Pd(111) (see Table II) having nine nearest neighbors.

The existence of fraction f_3^6 of uniformly located probes can be explained by a self-organizing process leading to probe positions close to the black spots in Fig. 4. A more cogent argumentation, taking into consideration the hyperfine fields, will follow in Sec. V C. However, a slight difference between V_{zz} of $f_3^6(E_6)$ and of $f_3^6(E_7)$ exists, which may originate from the different preparation techniques used in E_6 and E_7. The PAC time spectrum of experiment E_7 contains a second fraction, which exhibits the hyperfine parameter of a substitutional step site. It cannot be decided from the EFG whether these step sites are located in the first or in a second Pd layer created by possible 3*d* island growth. However, the assumption of a substitutional step site in the second layer will be supported later on, when the magnetic hyperfine fields from the different Pd layers are discussed. Therefore this fraction is labeled f_0^7.

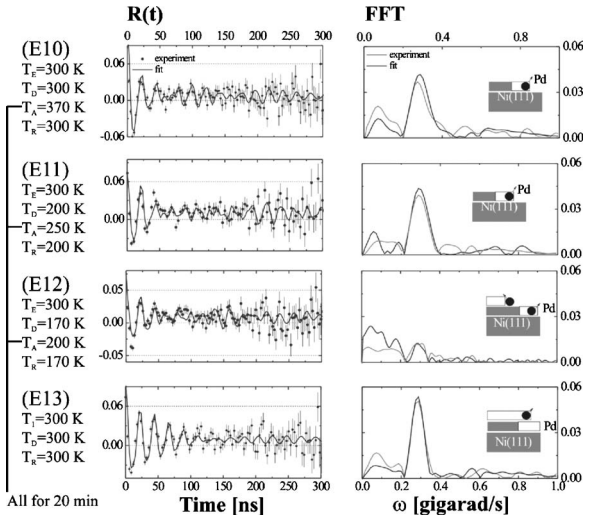

FIG. 9. PAC time spectra and the fast-fourier transforms (right graphs) of experiments E_{10}–E_{13}. T_D, T_A, and T_R denote the deposition, annealing and $R(t)$ recording temperature respectively. A structural model is indicated. For E_2 the two fractions of probes were numerically split in a simulation.

2. NN=9 and NN=12: Two monolayers of Pd

In experiment E_8, a Ni(111) surface—covered with one monolayer of Pd at T_E=300 K—was decorated with probe atoms at T_D=300 K. Thereafter, an additional Pd layer was evaporated at T_E^1=300 K. The PAC spectrum (Fig. 8) could be fitted using only one fraction f_0^9, corresponding to a substitutional terrace site with NN=9 in the uppermost Pd layer, since the asymmetry parameter of the electric-field gradient η is zero, the EFG points along the surface normal and the value of the EFG again is close to that of probes located in substitutional terrace sites on Pd(111).[11] This means that the probe atoms could not be trapped in the first Pd layer, but rather moved to the uppermost layer.

In experiment E_9 at a temperature of T_E^1=300 K, four additional monolayers of Pd were evaporated onto the sample prepared in experiment E_8. The PAC spectrum (Fig. 8) could be fitted using two fractions. Fraction $f_0^9(E_9)$ shows the EFG of a substitutional terrace site (cf. Table II and Fig. 6). It could not be determined in which layer the probes are located. Due to the preparation process it is most likely that a small amount of probes remained in the second uncovered layer. The second fraction f_0^{12} represents the probe atoms which are covered by Pd atoms with NN=12. The interpretation of its interaction frequency is not unambiguous and offers two possibilities.

(i) A pure quadrupole interaction (EFG) that results from defined local dislocations leads to low-frequency oscillations in the $R(t)$ spectrum. This option is rather improbable since there is no theoretical evidence for such dislocations–the probes are located in the second layer and not at the interface.

(ii) An almost pure magnetic dipole interaction is more likely: in that case a B_{hf} of 2.7 (2) T would be present at the Cd probe nucleus.

3. 5≤NN≤8: One monolayer of Pd

In order to realize step sites in a single Pd monolayer, the Ni(53,47,50) surface was initially decorated with 0.4 monolayers of Pd at T_E=300 K. In three different experiments after probe deposition the sample was annealed at 370 K (experiment E_{10}), 250 $K(E_{11})$ and 200 K (E_{12}). The PAC time spectra (Fig. 9) contain a fraction f_3^4 corresponding to a substitutional step site with NN=7. The asymmetry, V_{zz} and direction of the EFG corresponding to that site are almost equal to those on Pd(111) surfaces (Fig. 6).

In E_{11} an additional fraction f_3^5 occurs, showing hyperfine parameters thus far not observed at Ni and Pd surfaces. Due to the value of η and the direction of the EFG, which is similar to that of a kink site on Pd(111),[11] as well as the trend of the EFG (Fig. 6), it is suggested that this site corresponds to a substitutional kink site with NN=8 (Fig. 2). Obviously, an annealing temperature was chosen which was high enough to allow the probe atoms to enter the terraces via surface diffusion, but was low enough to prevent "flattening" of the kinks and cusps in the Pd layer.

In E_{12} (Fig. 9) an additional fraction f_3^2 occurs, showing hyperfine parameters differing from f_3^5 (Table II). It corresponds to the free step site (Fig. 6). This observation can be explained as follows.

In the experiments $E_{10}-E_{12}$, $c(13\times13)$Pd "wires" were grown along the steps on Ni(53,47,50), having a nominal width of 2 nm. The structure of the wires was analyzed by LEED—they showed no difference from one monolayer of Pd grown on Ni(111). Although in experiment E_{10} an annealing temperature of 370 K was chosen, no substitutional terrace sites in 0.4 monolayers deposited on Ni(53,47,50), could be observed, which apparently disagrees with the findings of Hunger[11] for a Pd(111) single crystal surface. Moreover, the mobility of the Pd atoms is much higher on Ni(111) than on Pd(111), as can be deduced from the fact that substitutional step sites already occur at T_A=200 K on Pd/Ni(111) and not at T_A=250 K as was found for Pd(111). This result can be explained from the larger lattice parameter of Pd (a_{NN}=2.75 Å) compared with that of Ni (a_{NN}=2.49 Å), offering the In (a_{NN}=3.25 Å) and Cd (a_{NN}=2.98 Å) probe atoms more space for relaxation. Therefore a "repulsive force" originating at the interface prevents the probes from penetrating the Pd terraces deeply. A similar behavior was found for the lateral direction: During evaporation of Pd onto Ni(111), the probe atoms are not covered in the Ni or first Pd layer, as was shown in experiment E_6 for 200 K and experiment E_8 for 300 K growth temperature. In fact, they are repelled from the Ni/Pd interface towards the Pd layer. If more then two monolayers are grown onto the Ni(111) surface, the probe atoms are covered even at 300 K growth temperature, as was shown in experiment E_9.

4. NN=7: Two monolayers of Pd

In E_7, substitutional step sites were observed, which could not be clearly assigned to the first or second Pd layer. Since the EFG is the same for both cases, the value of the magnetic hyperfine field has to be taken into account. Therefore in experiment E_{13}, 1.8 monolayers of Pd were evaporated onto the Ni(53,47,50) surface at T_E=300 K. At a temperature of T_D=300 K the ^{111m}Cd probes were deposited. The PAC time spectrum (Fig. 9) could be fitted using only one fraction f_3^4. It corresponds to the substitutional step site, but due to the preparation process the probes must be located in the second layer of Pd. Comparing the B_{hf} value of $f_3^4(E_7)[B_{hf}=0.9(5)\mathrm{T}]$ with that of $f_3^4(E_{13})[B_{hf}=0.7(5)\mathrm{T}]$, it is evident that the probes for $f_3^4(E_7)$ are located in the *second* Pd layer.

V. DISCUSSION

A. Ni(111) surface

The dependence of the magnetic hyperfine field B_{hf} on the coordination number at differently oriented surfaces is presented in Fig. 6. An almost monotonic increase of B_{hf} with decreasing number of nearest Ni neighbors can clearly be seen. However, the sign of B_{hf} was not measured, but deduced by comparison with theoretical results.[14–18] The surprisingly large differences in the magnetic hyperfine fields at the probe nuclei and the strong correlation between the B_{hf} values and the number of nearest Ni neighbors (NNs) require discussion. The correlation could be explained by modern density functional theory (DFT) calculations based on the Green's-function method.[16] and APW+lo method.[18] The underlying mechanism is given by the hybridization between spin-split electronic *d* bands of the nearest-neighbor atoms with the *s* states of the impurity, which leads to induced *s* moments responsible (at least to a large extent) for the magnetic hyperfine fields at the impurity. Moreover, the *sd* hybridization leads to a splitting of the *s*-electron density of states into bonding and antibonding peaks near the Fermi level.[33] Weaker hybridization for spin-up than for spin-down states in the bonding bands leads to a negative B_{hf} at Cd in Ni bulk. With reduced coordination, the peaks again split due to the *sp* hybridization, since *s* and *p* states are not decoupled if cubic symmetry is no longer present.[24] The band width decreases and hence the peak height increases. As a third effect, the position of the Fermi energy shifts. This leads to a dependence of B_{hf} on the coordination number NN. The DFT calculations also suggest that other elements should have a dependence which is different from that of Cd, and that deviations will be found on varying the magnetic substrate.[16,18]

Comparing Ni(001) and Ni(111) surfaces for NN=7,[13] and NN=4,[12,32] there is a strong indication that B_{hf} does not depend on the local symmetry but essentially on the number of nearest neighbors. A *vice versa* argumentation can be performed for the terrace sites: while substitutional terrace sites and adatoms show C_{4v}/C_{3v} symmetry on Ni(001),[12] and Ni(111), respectively, their magnetic hyperfine fields differ significantly from 7 to 16 T. These findings, as well as the measured EFG and B_{hf} on Ni(111), are in good agreement with theoretical calculations.[16–18] It was shown by Bellini and Cottenier *et al.*[17,18] that the spatial relaxation around the probe atoms plays a significant role for the magnetic hyperfine field present at the Cd nucleus, and that a realization of different NN by bulk vacancies would lead to the same trend as shown in Fig. 6, but to different maximal B_{hf} values.

Although the experiments of Refs. 2 and 3 are quite different from ours, it is worthwhile to perform a brief compari-

son: in Ref. 2 a small non monotonic increase of the magnetic spin moment with decreasing coordination number was reported for isolated Fe clusters on ultrathin Ni films by means of x-ray magnetic circular dichroism. In Ref. 3, small Co clusters were deposited onto a platinum surface. It was found that their anisotropy parameter K and the orbital moment L decrease—in a similar way to our findings for the hyperfine field—with increasing coordination number. The theoretical understanding of the magnetic properties of adatoms and small clusters on surfaces was given by Cabria *et al.*,[34] Lazarovits *et al.*,[35] and by Klautau *et al.*[36]

B. Pd on Ni(111)

The results of the measurements with mixed coordination numbers (Pd and Ni) are discussed together with Fig. 6. At the substitutional terrace site at a coverage of one monolayer Pd, the Cd nucleus experiences $B_{hf}=4.5(3)$ T, and $B_{hf}=1.0(8)$ T at a coverage of two monolayers of Pd. Pd is magnetically polarized by the ferromagnetic Ni substrate, resulting in a magnetic hyperfine field produced not only by the Ni but also by the Pd nearest neighbors. These results are similar to those for ultrathin Pd layers on Ni(001).[5]

Comparing the magnetic hyperfine fields B_{hf} at substitutional terrace sites of probe atoms located on the uncovered and on the Pd covered Ni(111) surface (NN=9), one finds that $|B_{hf}|$ decreases with increasing number of nearest Pd neighbors, while the total NN is kept constant. The same $|B_{hf}|$ trend holds for step sites with NN=8, NN=7, and NN=5. For comparison with theory, a system consisting of a Pd single crystal covered by one monolayer of Ni shows a magnetic moment of 0.24 μ_B per atom in the first Pd monolayer and 0.20 μ_B per atom in the second Pd monolayer, while the magnetic moment in the Ni interface layer is increased to 0.89 μ_B per atom, in comparison to the Ni bulk (0.6 μ_B per atom).[6]

An analogous behavior of $|B_{hf}|$ to that of the magnetic moment becomes evident if one considers that the magnetic moments of both the Ni and the polarized Pd atoms in the neighborhood of the probe atoms arise from *s-d* hybridization. This can be made evident by a simple comparison presented in Fig. 10: the total magnetic moment m_{total} of a cluster formed by the nearest-neighbor atoms (Ni and Pd) of the Cd probe atom was constructed by adding the calculated values. Only surface sites with equal total numbers of nearest neighbors can be taken into account, due to the sensitivity of the *s* density of states on the coordination number. A linear dependence of $|B_{hf}|$ and the computed magnetic moments (from the cluster of nearest neighbors), as shown in Fig. 10, is obtained with the assumption of a strongly enhanced magnetic moment of Pd-decorated Ni, with $m=0.89$ μ_B as calculated in Ref. 6.

C. Laterally structured surfaces

From the present work, access to periodically distributed isolated atoms on surfaces can be deduced. Stable positions of Cd probe atoms on the pure Ni surface were found for substitutional terrace sites where the impurities occupy the highest coordination number at the surface. Within these sites, the probe atoms are randomly distributed. A very different and interesting situation is formed when ultra thin Pd layers are evaporated onto the Ni surface. For coverage with 0.4 monolayers of Pd, a repulsive force coming from the lateral Ni/Pd interface prevents the "Pd wires" from being penetrated by the Cd probe atoms. Even at temperatures above 300 K, no terrace sites could be prepared in the first or second Pd layer. A stabilized ensemble of pure substitutional step sites of the probe atoms is present, although the mobility of the Pd atoms is much higher than on the Pd(111) single crystal surface. For a Ni surface covered by a *full* monolayer of Pd, impurity sites with different NN and local symmetry (Fig. 4) are obtained within the Pd layer due to the Moiré-like pattern of the interface layers. The result for the EFG, discussed in Sec. IV, allows for only one impurity site (with NN=9) and therefore implies a self-organized occupation of selected sites. Taking the hyperfine field into account, we obtain substantial support for the following conclusions:

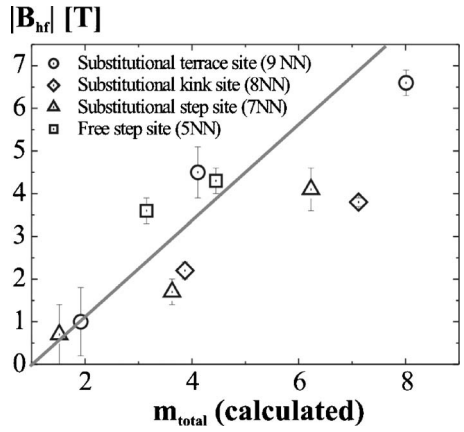

FIG. 10. Magnetic hyperfine field B_{hf} vs the calculated total magnetic moment of the cluster of nearest neighbors. The moment m_{total} was constructed by addition of the contributions from every atom belonging to the cluster formed by the nearest neighborhood of the probe atom, e.g., 0.89 μ_B from Ni atoms at the Ni/Pd interface, 0.6 μ_B from the Ni bulk, 0.24 μ_B from the first Pd monolayer, and 0.20 μ_B from the second Pd monolayer with respect to the interface (Ref. 6).

Firstly, in the PAC spectra of E_6 and E_7 only *one* discrete fraction could be resolved which could be attributed to a substitutional terrace site. No other discrete fractions exist. Second, a broad distribution of B_{hf} between 4.5 T (9 NN) and 1.7 T (7 NN taken from E_{10}) would lead, even if a constant EFG for all occupied sites is assumed, to the destruction of the beat pattern resulting from the discrete magnetic hyperfine field as shown in the simulation of Fig. 8. Therefore only one surface site (with NN=9) is occupied by a considerably large fraction of Cd probe atoms. The $c(13\times13)$Pd/Ni(111) interface thus behaves similarly to the $c(16\times2)$Pd/Ni(001) interface analyzed in previous experiments.[5] Figures 4(b) and 4(c) illustrate a noteworthy difference between the two cases: For Pd on Ni(111), the atoms or clusters would be arranged within a regular hexagonal array separated by ~2 nm. In contrast, for Pd on Ni(001) surfaces, the impurity atoms are very close to each other in

one direction (~0.5 nm) and separated from each other in the other direction (~4 nm), giving rise to the formation of separated lines.

VI. SUMMARY AND CONCLUSIONS

A Ni(111) and a Ni(53,47,50) vicinal single-crystal surface were analyzed using perturbed angular correlation spectroscopy (PAC) of isolated ^{111}In/^{111}Cd and ^{111m}Cd/^{111}Cd probe isotopes deposited by a soft landing technique. Due to the surface roughness (terraces, steps, kinks, etc.), various adsorption sites are available to the probe atoms. Every site shows a distinct number of nearest neighbors (NNs) and can be occupied with a probe atom by means of surface diffusion forced by annealing. Measuring the magnetic hyperfine field B_{hf} for each fraction of probe atoms located at certain sites, we found that with decreasing number of nearest Ni neighbors (NNs), the magnetic hyperfine field increases in the range from $B_{hf}=-7$ T for NN=12 to $B_{hf}=16$ T for NN=3. B_{hf} depends mainly on the coordination number and not on the local symmetry of the nearest Ni neighbors.

In a second series of experiments, ultrathin layers of Pd deposited onto the surface of a Ni(111) and Ni(53,47,50) single crystal were analyzed by LEED and PAC spectroscopy. It was found that at room temperature, one monolayer of Pd grows in a $c(13\times13)$ orientation which corresponds to a vertically corrugated (111) orientation of the Pd terraces. Using ^{111}In/^{111}Cd and ^{111m}Cd/^{111}Cd isotopes as probes, the magnetic hyperfine fields were measured with atomic resolution at various sites of the interface. While keeping the number of monolayers constant but varying the number of Pd nearest neighbors, B_{hf} shows the same trend as on an uncovered Ni(111) surface. While keeping the total number of nearest neighbors constant but varying the stoichiometric composition, i.e., the fraction of Pd and Ni atoms, the magnetic hyperfine field reflects the trend (enhancement) of the magnetic moment shown by Blügel.[6]

Due to the incommensurate $c(13\times13)$ structure of one monolayer Pd grown on Ni(111), every substitutional site of the surface shows a different arrangement of the nearest-neighbor atoms, leading to regions with NN=7–NN=9. The weak damping of the respective PAC spectra and the discrete B_{hf} value allow only one interpretation: the Cd probes occupy the substitutional sites selectively, achieving the highest coordination and thus confirming earlier observations on the Pd/Ni(001) interface, where also only one site (NN=10) was occupied.[5] The reason for this self-organized selection of surface sites lies in the different sizes of the elements involved.

Besides the structural aspects, PAC allows the measurement of the magnetic hyperfine field at the nuclei of an ensemble of atoms located on specified uniform sites at the surface. Although a direct and easy calculation of the local moment from the magnetic hyperfine field cannot be given, B_{hf} roughly reflects the trend one also would expect from the magnetic moment, e.g., a drastic change upon the reduction of the coordination number due to band narrowing or splitting and a decrease with increasing distance from the interface with a ferromagnetic material. One reason for that is the magnetically passive nature of the probe atom Cd that shows a filled *d* shell with states deeply below the Fermi level. Thus the magnetic hyperfine filed at the nucleus originates exclusively from the magnetic host.

While in the systems mentioned above the electric transport is based on both the *d* and the *sp* electrons, e.g., the ferromagnetic properties have itinerant character, materials that are doped or alloyed with *d* or *f* elements exhibiting localized moments can be investigated with respect to the magnetic coupling and the polarization of the conducting electrons by PAC. Recently this was performed for rare-earth-indium compounds,[38] ferromagnetic spinel semiconductors,[39] or CMR manganites.[40] Nuclear probe methods like PAC and PAD (perturbed angular distribution) are also very well suited for the investigation of diluted magnetic systems on the magnetically active[41] or passive sites. Thus the upcoming new class of spintronics devices basing on dilute magnetic systems can be explored using nuclear probe methods like PAC.

The ultimate goal in data storage technology is the use of very small clusters or even single atoms as "bits." Since the *s*-electron polarization is probably not a practicable parameter, e.g., for information carriers in computer technology, other kinds of "probe" atoms have to be used. In particular, atoms or clusters with a high magnetic anisotropy, such as rare earths, may be placed in the surface sites. The coupling of such $5d(4f)$ impurity atoms embedded in a Pd layer of $4d$ atoms on a ferromagnetic substrate with $3d$ atoms should be studied in order to find out whether the rare-earth atoms at their selected sites may even occupy two or more suitable stable states, e.g., due to valence variation. Preliminary experiments with ^{147}Gd decaying to ^{147}Eu are being performed with ASPIC/ISOLDE. In our PAC experiments with radioactive atoms, the γ-ray counter capacity does not allow for more than 10^{11} probe atoms per sample, although a 1-cm^2 sample surface has the capacity of 10^{13} probe atoms. Investigations with stable atoms, applying scanning tunneling microscopy, should reveal whether the majority of the 10^{13} sites per cm^2 can be occupied, i.e., whether an ordered structure of isolated impurities is obtained. These investigations are in progress.

ACKNOWLEDGMENTS

The authors would like to thank Valerio Bellini, Christian Abromeit and Jürgen Bosse for fruitful discussion and William D. Brewer for critical reading. M. D. acknowledges the financial support by the BMBF (Grant No.05 KK1TSA/7). This work was supported by the European Commission (Grant No.HPRI-CT-1998-00018).

[1] G. Binasch, P. Grünberg, F. Saurenbach, and W. Zinn, Phys. Rev. B **39**, 4828 (1989).
[2] J. T. Lau, A. Fohlisch, R. Nietuby, M. Reif, and W. Wurth, Phys. Rev. Lett. **89**, 057201 (2002).
[3] P. Gambardella, S. Rusponi, M. Veronese, S. S. Dhesi, C. Grazioli, A. Dallmeyer, I. Cabria, R. Zeller, P. H. Dederichs, K. Kern, C. Carbone, and H. Brune, Science **300**, 1130 (2003).
[4] U. Gradmann and R. Bergholz, Phys. Rev. Lett. **52**, 771 (1984).
[5] H. H. Bertschat, H.-H. Blaschek, H. Granzer, K. Potzger, S. Seeger, W.-D. Zeitz, H. Niehus, A. Burchard, and D. Forkel-Wirth (ISOLDE Collaboration), Phys. Rev. Lett. **80**, 2721 (1998).
[6] S. Blügel, Europhys. Lett. **7**, 743 (1988).
[7] P. H. Dederichs, P. Lang, K. Willenborg, R. Zeller, N. Papanikolaou, and N. Stefanou, Hyperfine Interact. **78**, 341 (1993).
[8] M. Gsell, P. Jakob, and D. Menzel, Science **280**, 717 (1998).
[9] K. Potzger, A. Weber, H. H. Bertschat, W.-D. Zeitz, and M. Dietrich, Phys. Rev. Lett. **88**, 247201 (2002).
[10] R. Fink, B.-U. Runge, K. Jacobs, G. Krausch, J. Lohmüller, B. Luckscheiter, U. Woehrmann, and G. Schatz, J. Phys.: Condens. Matter **5**, 3837 (1993).
[11] E. Hunger and H. Haas, Surf. Sci. **234**, 273 (1990).
[12] J. Voigt, R. Fink, G. Krausch, B. Luckscheiter, R. Platzer, U. Wöhrmann, X. L. Ding, and G. Schatz, Phys. Rev. Lett. **64**, 2202 (1990); J. Voigt, Ph.D. thesis, University of Konstanz, Konstanz, 1990.
[13] H. Granzer, H. H. Bertschat, H. Haas, W.-D. Zeitz, J. Lohmüller, and G. Schatz, Phys. Rev. Lett. **77**, 4261 (1996).
[14] B. Lindgren and H. Ghandour, Hyperfine Interact. **78**, 291 (1993).
[15] B. Lindgren, Z. Naturforsch, Z. Naturforsch., A: Phys. Sci. **57a**, 544 (2002).
[16] Ph. Mavropoulos, J. Phys.: Condens. Matter **15**, 8115 (2003).
[17] S. Cottenier, V. Bellini, M. Cakmak, F. Manghi, and M. Rots, Phys. Rev. B **70**, 155418 (2004).
[18] V. Bellini, S. Cottenier, M. Cakmak, F. Manghi, and M. Rots, Phys. Rev. B **70**, 155419 (2004).
[19] E. Kugler, and D. Fiander, and B. Jonson, Nucl. Instrum. Meth. B **70**, 41 (1992).
[20] C. DeW. van Siclen, Phys. Rev. B **51**, 7796 (1995).
[21] S. Terada, T. Yokoyama, N. Saito, Y. Okamoto, and T. Ohta, Surf. Sci. **433-435**, 657 (1999).
[22] J. D. Jackson, *Classical Electrodynamics*, 3rd edition (John Wiley & Sons, New York, 1998).
[23] W. Nolting, *Quantentheorie des Magnetismus* (Teubner, Leipzig, 1997).
[24] Ph. Mavropoulos, N. Stefanou, B. Nonas, R. Zeller, and P. H. Dederichs, Phys. Rev. Lett. **81**, 1505 (1998).
[25] L. Boström, E. Karlsson, and S. Zetterlund, Phys. Scr. **2**, 65 (1970).
[26] G. Schatz and A. Weidinger, *Nukleare Festkörperphysik* (Teubner, Stuttgart, 1997).
[27] H. Gabriel and J. Bosse, in *Proceedings of the International Conference on Angular Correlations in Nuclear Disintigration, Delft, 1970* edited by H. van Krugten (Rotterdam University Press, 1971), p. 394–426.
[28] H. Frauenfelder and R. M. Steffen, *Angular Distribution of Nuclear Radiation in Alpha-, Beta-, and Gamma ray Spectroscopy*, edited by Kai Siegbahn (North-Holland, Amsterdam, 1965).
[29] H.-J. Stöckmann, *Dichtematritzen und Irreduzible Tensoren*, scripts from Marburg University (Marburg, 1991).
[30] B. Lindgren, Hyperfine Interact. **1**, 613 (1996).
[31] *Table of Isotopes*, edited by R. B. Firestone and V. S. Shirley 8th ed. (Wiley & Sons, New York, 1996); $Q_N(^{111}\mathrm{Cd})$ from R. Vianden, Hyperfine Interact. **15/16**, 1081 (1983).
[32] M. J. Prandolini, Y. Manzhur, A. Weber, K. Potzger, H. H. Bertschat, H. Ueno, H. Miyoshi, and M. Dietrich, Appl. Phys. Lett. **85**, 76 (2004).
[33] J. Kanamori, H. K. Yoshida, and K. Terakura, Hyperfine Interact. **9**, 363 (1981).
[34] I. Cabria, B. Nonas, R. Zeller, and P. H. Dederichs, Phys. Rev. B **65**, 054414 (2002).
[35] B. Lazarovits, L. Szunyogh, and P. Weinberger, Phys. Rev. B **65**, 104441 (2002).
[36] A. B. Klautau and S. Frota-Pessôa, Surf. Sci. **497**, 385 (2002).
[37] G. N. Rao, Hyperfine Interact. **7**, 141 (1979).
[38] M. Forker, R. Musseler, S. C. Bedi, M. Olzon-Dionysio, and S. D. de Souza, Phys. Rev. B **71**, 094404 (2005).
[39] V. Samokhvalov, S. Unterricker, I. Burlakova, F. Schneider, M. Dietrich, V. Tsurkan, and I. M. Tiginyanu, J. Phys. Chem. Solids **64**, 2069 (2003).
[40] J. P. Araujo, J. G. Correia, V. S. Amaral, P. B. Tavares, F. Lencart-Silva, A. A. C. S Lourenco, J. B. Sousa, J. M. Vieira, and J. C. Soares, Hyperfine Interact. **133**, 89 (2001).
[41] R. Kirsch, M. J. Prandolini, M. Gierlings, M. Gruyters M, W. D. Brewer, and D. Riegel, J. Magn. Magn. Mater. **272**, 760 (2004).